



Dielectric and ferroelectric behaviour of Zr-doped BaTiO₃ perovskites

Qi Xu*, Zihan Li

College of Materials and Chemistry & Chemical Engineering, Chengdu University of Technology, Chengdu 610059, China

Received 31 December 2019; Received in revised form 20 April 2020; Accepted 16 June 2020

Abstract

The crystal structure, microstructure, dielectric and ferroelectric behaviour of Ba(Zr_xTi_{1-x})O₃ ($x = 0.05, 0.10, 0.15, 0.20, 0.25$) perovskites fabricated by high-temperature solid state method were investigated. Zr⁴⁺ ions are dissolved completely into B-site of the matrix BaTiO₃ within the studied composition range, leading to an expansion of the lattice. The average grain size decreased with Zr content increasing. In P-E loops, the remanent polarization gradually decreased with Zr-doping, indicating the depression of ferroelectricity. Temperature dependent dielectric properties at different frequencies exhibited obvious relaxor behaviour. It was shown that diffuseness coefficient γ increased from 1.45 ($x = 0.05$) to 1.89–1.90 ($x = 0.10$ – 0.25) by using the modified Curie-Weiss law for the fit. The permittivity of the Ba(Zr_xTi_{1-x})O₃ ceramics at room temperature was largely improved by Zr-doping, thus when $x = 0.20$, ϵ_r (1 kHz) = 10790.

Keywords: Zr-doping, BaTiO₃, perovskites, dielectric properties, relaxor

I. Introduction

Ba(Zr,Ti)O₃ was firstly investigated in 1950s as transducer material [1]. In the past almost 70 years, the subject has been very popular and studied a lot because Ba(Zr,Ti)O₃ has significant application in electronic industry, such as multi-layer ceramic capacitor (MLCC) dielectrics, resistors, transducers, thermal sensors, etc. [2,3]. With the rapid expansion of modern industry, electronic parts and components are developing towards the characteristics of precision and integration [4]. To meet these requirements, exploiting dielectric materials with high permittivity and favourable temperature stability is of critical importance.

For pure BaTiO₃, permittivity at room temperature is lower than 3000 and the dielectric temperature stability is poor due to its phase transformations at –80, 0 and 125 °C, while the maximum permittivity at the Curie temperature ($T_C \approx 125$ °C) can reach 7000 [5]. Thus, shifting T_C to lower temperature would be in favour of improving the dielectric constant at room temperature and broadening of the stable temperature range. Doping in either A-site or B-site of ABO₃-type perovskites has been commonly used for dielectric modification. A-site substitutions in BaTiO₃ ceramics in-

clude Sr²⁺, Ca²⁺, Mg²⁺, etc. [6–8]. B-site substitutions include Hf⁴⁺, Sn⁴⁺, Zr⁴⁺, Ta⁵⁺, Nb⁵⁺, etc. [9–13]. For these doped barium titanate ceramics, dielectric behaviour varies with doping concentration. According to literature reports, introduction of B-site ion is effective in lowering T_C [14]. Therefore, in the present work, B-site iso-valent substitution was investigated. Ti⁴⁺ is displaced by Zr⁴⁺. The effects of Zr⁴⁺ ions on the crystal structure, ferroelectric and dielectric behaviour of modified barium titanate ceramics were comprehensively studied. The emphases were placed on the shifting efficiency of the Curie point by Zr-doping in Ba(Zr,Ti)O₃ ceramics and the possibility of their application as capacitor dielectric materials.

II. Experimental

Ba(Zr_xTi_{1-x})O₃ ($x = 0.05, 0.10, 0.15, 0.20, 0.25$) ceramic samples were prepared by traditional solid-state reaction method. First, the raw powders BaCO₃ (purity 99.0%), ZrO₂ (purity 99.0%) and TiO₂ (purity 98.5%) were mixed stoichiometrically and ball milled with zirconium media in ethanol for 24 h. After drying at 100 °C, the powder mixture was calcined at 1150 °C for 2 h and subsequently ball-milled again for 24 h. Then, the powders were pressed into pellets of 12 mm in diameter and 1 mm in thickness under an uniaxial pressure of

* Corresponding authors: tel: +91 9861406462, e-mail: xuqi17@cdut.edu.cn

~200 MPa. The pellets were sintered at 1250–1400 °C for 2 h.

Phase structure was determined using X-ray powder diffraction (Cu K α radiation, PANalytical X'Pert PRO, Eindhoven, The Netherlands) operated at 40 kV and 40 mA. The microstructure of the ceramics was taken by scanning electron microscope (Quanta 450 FEG, FEI) on the cross-section. The average grain size was determined by the linear intercept method. Electrodes were fabricated with fire-on silver paste at 500 °C for 15 min. The dielectric properties were measured using a custom designed furnaces with a heating rate of 2 °C/min connected to a precision LCR meter (E4980A, Agilent, Santa Clara, USA) and computerized controlled data collection systems. To determine the ferroelectric properties, the sintered samples were polished to a thickness of 0.3 ± 0.02 mm and then the test was performed using a ferroelectric material test system (HVI0403-239, Radiant Technology, USA) in a silicone oil bath at 10 Hz.

III. Results and discussion

The bulk densities of the Ba(Zr $_x$ Ti $_{1-x}$)O $_3$ ceramics are shown in Figure 1 as a function of sintering temperature. For all the samples, the bulk densities first increased and then decreased with sintering temperature. Bulk density is one of the indexes to measure the sintering degree of ceramics. In this research, the sintering temperature of 1250 °C was too low so that the grain boundaries moved slowly and grain growth was incomplete. This led to the ceramic samples with relatively low bulk density. With the sintering temperature increasing up to 1300–1350 °C, the mass transfer process can be fully carried out, which is favourable for pores elimination, leading to increased bulk density. However, when the sintering temperature was too high (≥ 1400 °C), the pores were easily enclosed in the grain since the grain boundary moving rate was higher than the pores moving rate, leading to decreased bulk density of the ceramic sample. Thus, dense ceramics can be obtained in the range of 1300–1350 °C.

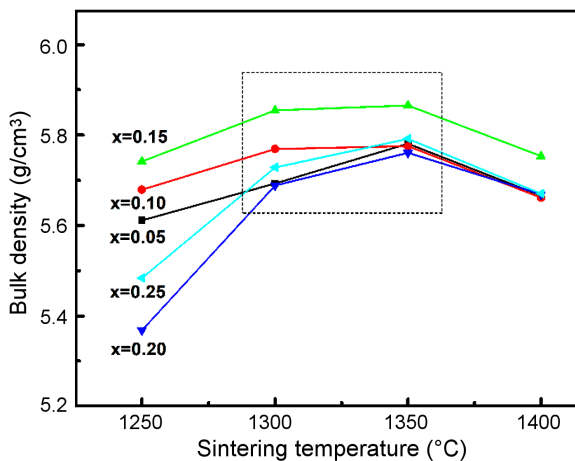


Figure 1. Bulk density of Ba(Zr $_x$ Ti $_{1-x}$)O $_3$ ceramics as a function of sintering temperature

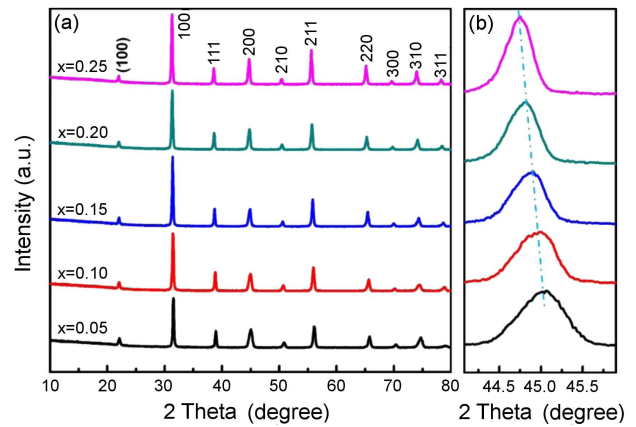


Figure 2. XRD patterns of Ba(Zr $_x$ Ti $_{1-x}$)O $_3$ ceramics sintered at 1350 °C: a) $2\theta = 10\text{--}80^\circ$ and b) $2\theta = 44\text{--}46^\circ$

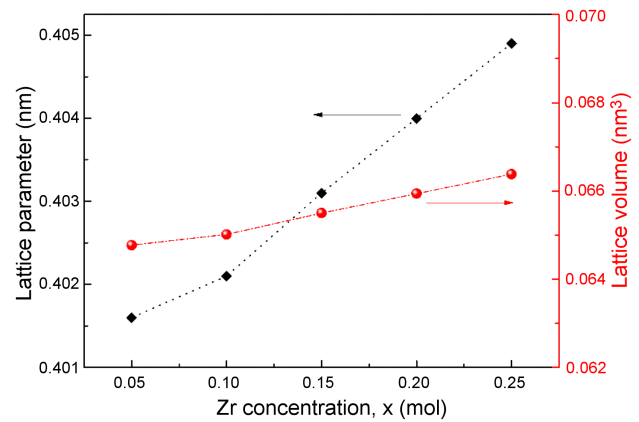


Figure 3. Lattice parameters and volumes as a function of Zr concentration

Figure 2 shows the XRD patterns of the sintered Ba(Zr $_x$ Ti $_{1-x}$)O $_3$ ceramic samples. All the compositions exhibited single pseudo-cubic perovskite structure and no secondary phase was observed. With the increase of Zr content, the diffraction peaks shifted to lower angle, as shown in the enlarged patterns of $2\theta = 44\text{--}46^\circ$ in Fig. 2b. Figure 3 shows the calculated lattice parameters and volumes of the Ba(Zr $_x$ Ti $_{1-x}$)O $_3$ ceramic samples. The lattice parameter increased from 0.402 to 0.405 nm when Zr concentration increases from $x = 0.05$ to $x = 0.25$. Correspondingly, the cell volume increased from 0.0648 nm 3 to 0.0664 nm 3 . According to Shannon's effective ionic radii with a coordination number of six [15], the radius of Zr $^{4+}$ is 0.72 Å, while Ti $^{4+}$ is 0.605 Å. The substitution of Zr $^{4+}$ to Ti $^{4+}$ leads to the expansion of the lattice, which is also responsible for the XRD peak shift. In addition, pure phase structure and shifting of the diffraction peak suggested that Zr $^{4+}$ ions are dissolved completely into B-site of the matrix BaTiO $_3$ within the studied composition range.

SEM images of the Ba(Zr $_x$ Ti $_{1-x}$)O $_3$ ceramics sintered at 1350 °C were illustrated in Fig. 4. Nearly no pores were observed and the average grain sizes of the ceramics with $x = 0.05, 0.10, 0.15, 0.20, 0.25$ were determined to be about 5.21, 5.04, 4.57, 4.40, 4.03 μm , re-

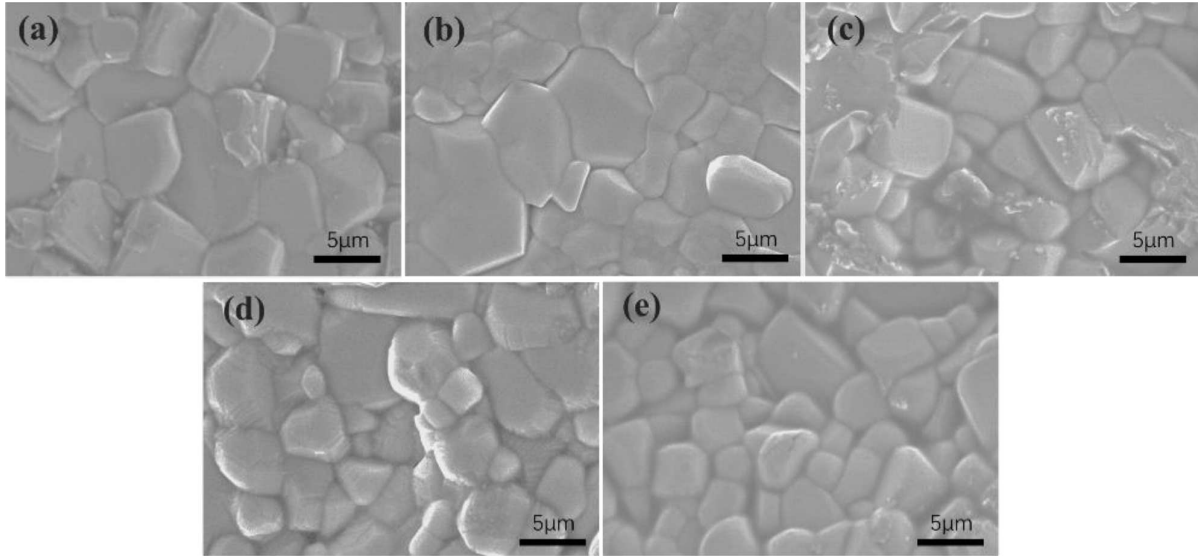


Figure 4. SEM images of $\text{Ba}(\text{Zr}_x\text{Ti}_{1-x})\text{O}_3$ ceramics: a) $x = 0.05$, b) $x = 0.10$, c) $x = 0.15$, d) $x = 0.20$ and e) $x = 0.25$

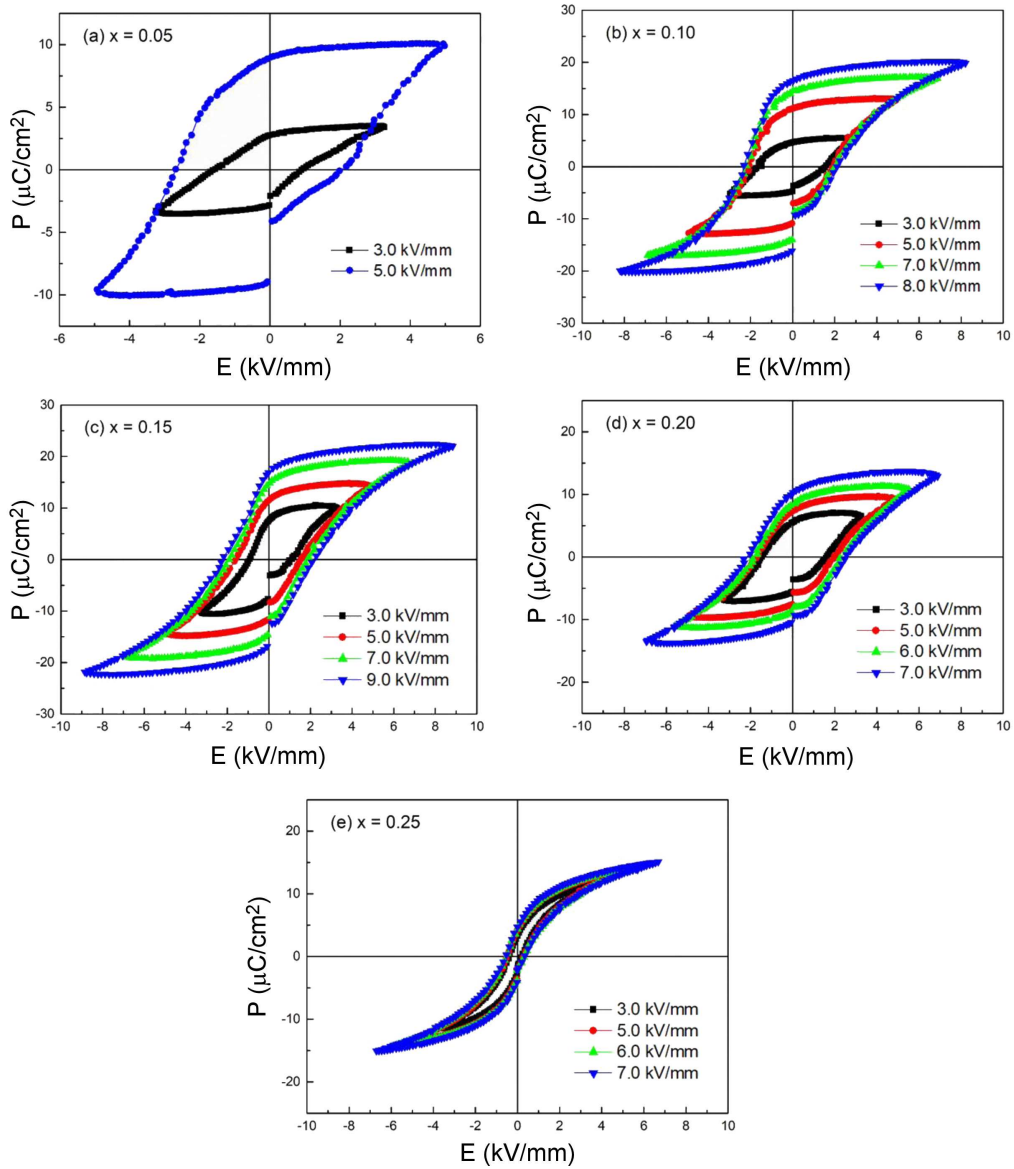


Figure 5. P - E loops of $\text{Ba}(\text{Zr}_x\text{Ti}_{1-x})\text{O}_3$ ceramics under different electric fields before breakdown

spectively. The values are close to literature reports for Ba(Zr,Ti)O₃ ceramics prepared by solid state method [16–18]. However, for the Ba(Zr,Ti)O₃ ceramics prepared by wet-chemical method, the grain size is much smaller [19]. The decline of grain size with Zr content was believed to be related to the ion mobility [20]. Since the radius of Zr⁴⁺ (0.72 Å) is larger than Ti⁴⁺ (0.605 Å), the ion mobility reduced with the increase of Zr content, which depressed grain boundary migration, leading to the decrease of grain size.

Figure 5 displays the *P-E* loops of the Ba(Zr_xTi_{1-x})O₃ ceramics sintered at 1350 °C under different electric fields at 10 Hz and room temperature. In all the compositions, the polarization gradually increased with the increase of electric field. For $x = 0.05$, the *P-E* loops exhibited typical ferroelectric characteristics. For $x = 0.10$ – 0.15 , the maximum polarization (P_m) largely enhanced ($\sim 20 \mu\text{C}/\text{cm}^2$ at 8 kV/mm) and the remanent polarization (P_r) remained around $17 \mu\text{C}/\text{cm}^2$. For $x = 0.25$, P_r reduced to $4.9 \mu\text{C}/\text{cm}^2$ at 6.7 kV/mm. The *P-E* loops became gradually depressed with Zr-doping, demonstrating obvious relaxation behaviour.

To evaluate the potential for application of the Ba(Zr_xTi_{1-x})O₃ ceramics for capacitive storage systems, the energy-storage density (W) was calculated from *P-E* loops using the formula [21]:

$$W = \int_0^E E dP \quad (1)$$

Figure 6 shows the maximum recoverable energy-storage density of the Ba(Zr_xTi_{1-x})O₃ ceramic samples under critical electric field. For the compositions with $x = 0$ – 0.20 , energy-storage density was no more than $0.15 \text{ J}/\text{cm}^3$ due to the large remanent polarization P_r . When $x = 0.25$, W increased to $0.2 \text{ J}/\text{cm}^3$ under 6.7 kV/mm. Even though the value was enhanced compared to pure BaTiO₃, the energy-storage density of Ba(Zr_xTi_{1-x})O₃ ceramics was still lower than other

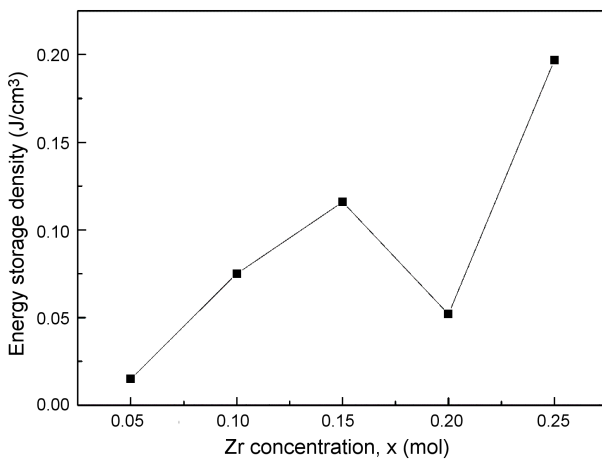


Figure 6. Maximum energy-storage density of Ba(Zr_xTi_{1-x})O₃ ceramics

ceramic systems [22–25]. Enhancing the breakdown strength of Ba(Zr,Ti)O₃-based ceramics was reported to be an effective method for improving the energy-storage performance [26], which would be investigated in our future work.

Figure 7 presents the dielectric constant and dielectric loss as a function of temperature at different frequencies (0.1 kHz, 1 kHz, 10 kHz, 100 kHz) for the Ba(Zr_xTi_{1-x})O₃ ceramics. In Fig. 7a, two permittivity peaks at T_1 and T_m were observed in the temperature dependent dielectric constant curves. It is known that for pure BaTiO₃ ceramics, the transition temperatures of cubic paraelectric \rightarrow tetragonal \rightarrow orthorhombic phase are $T_m \approx 125 \text{ }^\circ\text{C}$ and $T_1 = 5 \text{ }^\circ\text{C}$, respectively [27]. With initial Zr-doping, T_1 shifted to higher temperature while T_m shifted to lower side. For $x = 0.05$, $T_1 = 55 \text{ }^\circ\text{C}$ and $T_m = 99 \text{ }^\circ\text{C}$. Mahajan *et al.* [28] measured the dielectric behaviour of La³⁺ doped BaZr_{0.05}Ti_{0.95}O₃ ceramics and reported that two dielectric peaks in pure BaZr_{0.05}Ti_{0.95}O₃ merged with lanthanum doping, which also well supported our results. With further increase of Zr content, the two peaks merged into one broad peak and T_m kept moving to lower temperature, as shown in Fig. 7b–d. For the sample with $x = 0.25$, T_m was even lower than $20 \text{ }^\circ\text{C}$. Thus, no dielectric peak appeared in Fig. 7e. Figure 8 shows the shift of T_m as a function of Zr-doping. The shifting efficiency was calculated to be $\sim 4.5 \text{ }^\circ\text{C}/(\text{mol}\% \text{ Zr})$, which means that the Curie point would reduce $\sim 4.5 \text{ }^\circ\text{C}$ when Ti⁴⁺ is replaced by 1 mol% Zr⁴⁺ in B-site. The result is consistent with previous reports [14]. Zr⁴⁺ is proved to be an effective dopant for shift of the Curie peak, which can be widely employed in modifying dielectric performance of perovskites [29,30].

From Fig. 7, obvious relaxor behaviour was found along with the permittivity anomaly. The modified Curie-Weiss law can be used to describe the diffuse phase transition and relaxor characteristics:

$$\frac{1}{\varepsilon} - \frac{1}{\varepsilon_m} = \frac{(T - T_m)^\gamma}{C} \quad (2)$$

where ε and ε_m are the permittivity and maximum permittivity, respectively; C is analogous to the Curie constant; γ is the diffuseness coefficient. For ideal ferroelectric relaxors, $\gamma = 2$ and for normal ferroelectrics, $\gamma = 1$. Figure 9 shows the plots of $\ln(1/\varepsilon_r) - (1/\varepsilon_m)$ as a function of $\ln(T - T_m)$ for the Ba(Zr_xTi_{1-x})O₃ ceramics at 1 kHz. Diffuseness coefficient γ was determined from the slope. The fitting curves of all the samples exhibited linear characteristics. γ value was calculated to be in the range of 1–2, demonstrating the relaxor ferroelectric feature of the Ba(Zr_xTi_{1-x})O₃ ceramics. For the samples with low Zr content ($x = 0.05$), $\gamma = 1.45$. For the composition with higher Zr content ($0.10 \leq x \leq 0.25$), γ increased to 1.89–1.90. Zr-doping enhanced the relaxor behaviour, which was consistent with the above ferroelectric hysteresis loops analysis.

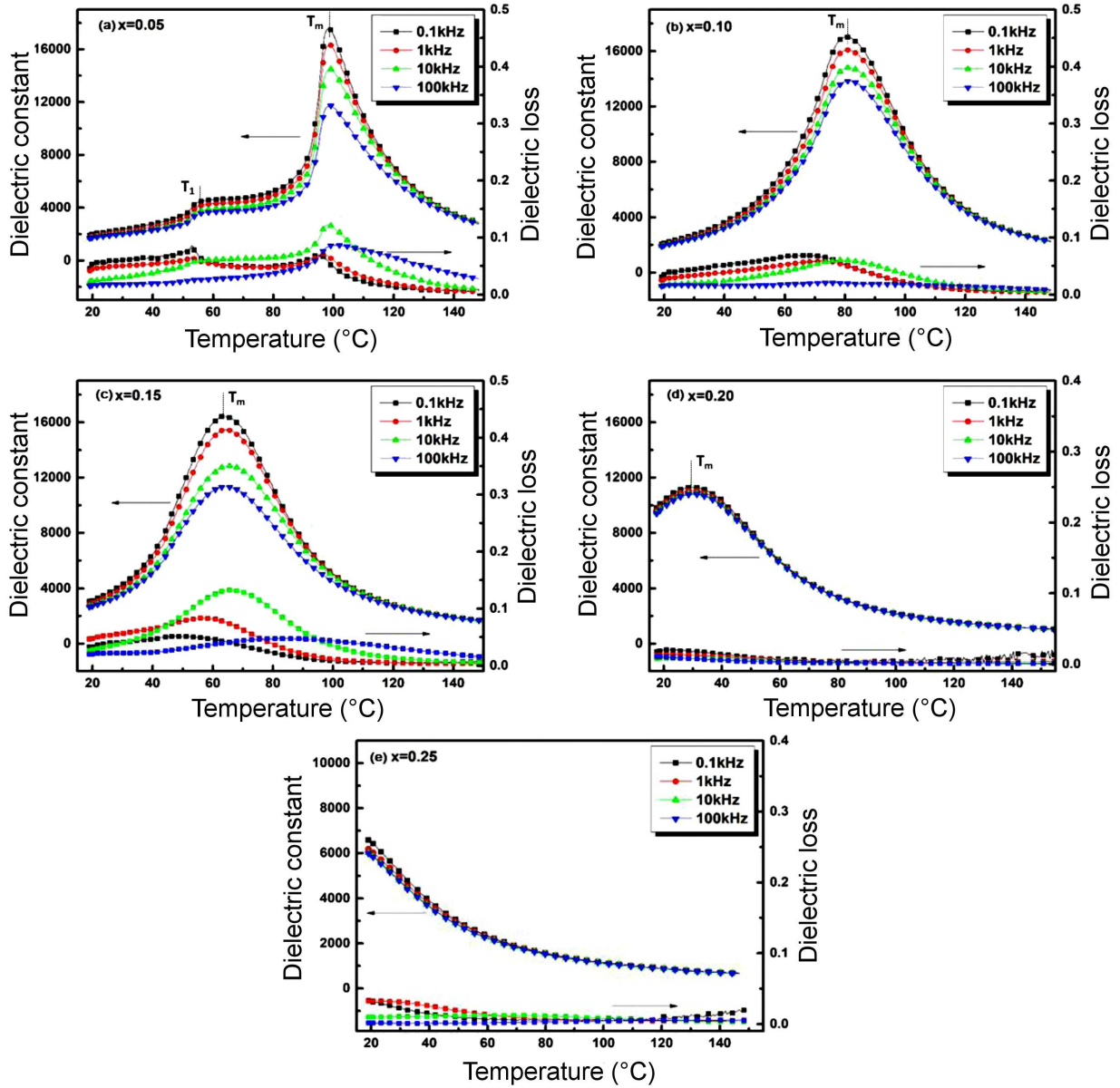


Figure 7. Dielectric constant and dielectric loss as a function of temperature measured at frequencies from 0.1 kHz to 100 kHz for Ba(Zr_xTi_{1-x})O₃ ceramics

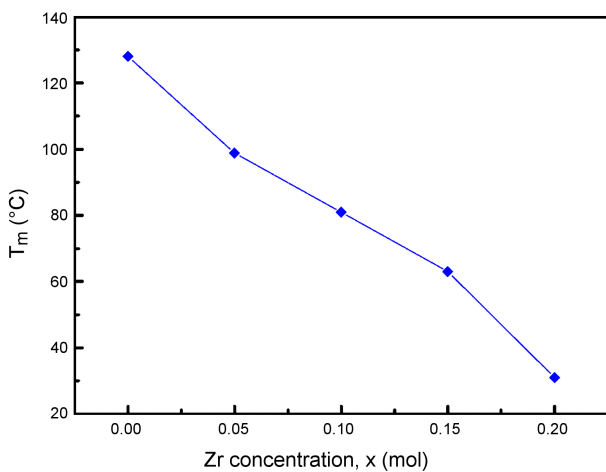


Figure 8. The shift of T_m (1 kHz) as a function of Zr-doping content

The dielectric properties of the Ba(Zr_xTi_{1-x})O₃ ceramics at room temperature were listed in Table 1. The permittivity gradually increased with the increase of Zr content. For the composition with x = 0.20, ε_r sharply increased to over 10500 at both 1 kHz and 100 kHz. However, further introduction of Zr restrained dielectric properties. When x = 0.25, the permittivity reduced to

Table 1. Dielectric properties of Ba(Zr_xTi_{1-x})O₃ ceramics at room temperature (25 °C)

x	ε _r	tan δ	ε _r	tan δ
	(1 kHz)	(1 kHz)	(100 kHz)	(100 kHz)
0.05	2035	0.048	1870	0.017
0.10	2325	0.031	2200	0.016
0.15	3450	0.053	3100	0.021
0.20	10790	0.013	10540	0.009
0.25	5515	0.033	5330	0.001

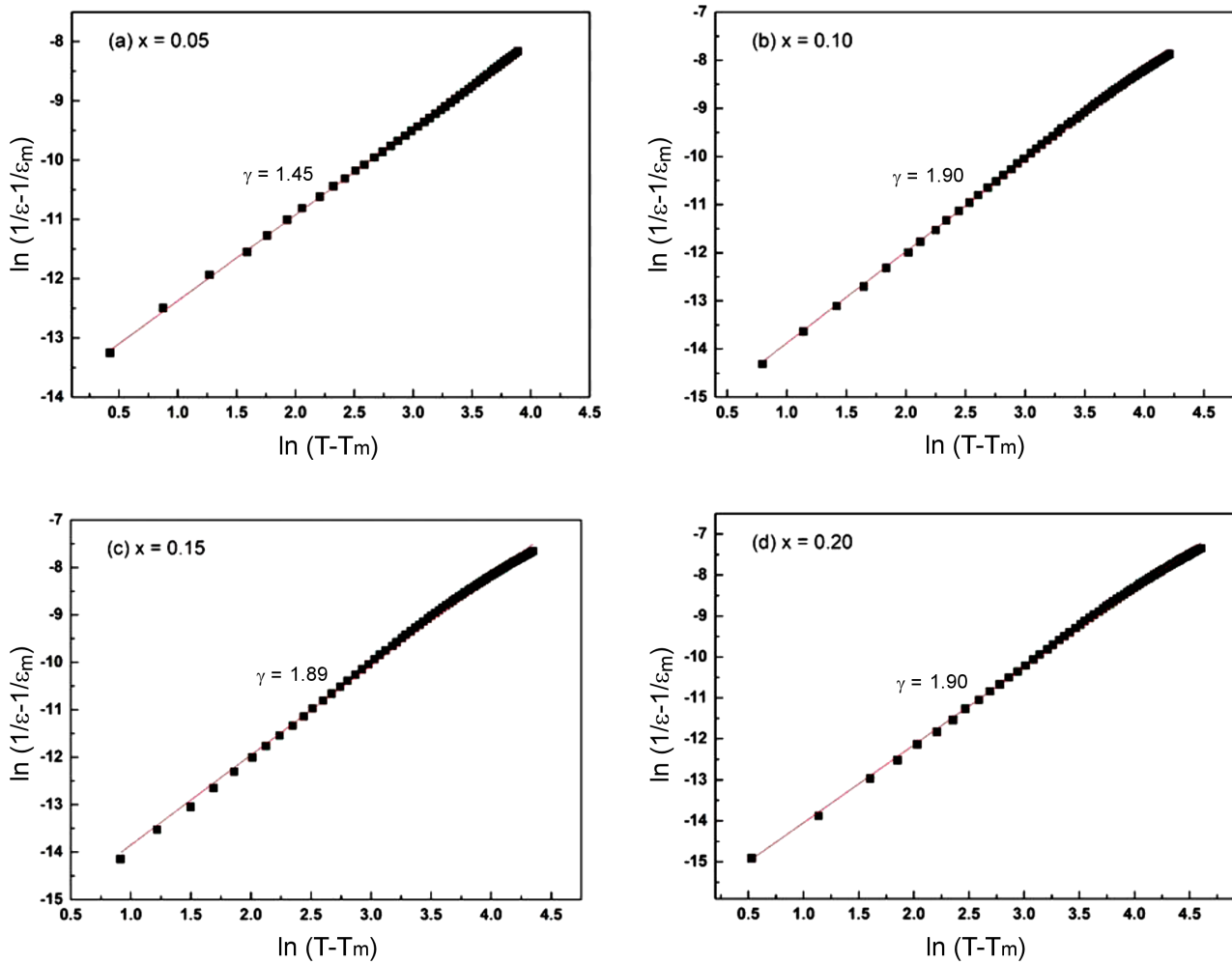


Figure 9. Plots of $\ln(1/\varepsilon - 1/\varepsilon_m)$ versus $\ln(T - T_m)$ at 1 kHz

5515 at 1 kHz and 5330 at 100 kHz. The variation of dielectric constant at room temperature was related to the Curie point shift effect by Zr addition.

IV. Conclusions

$\text{Ba}(\text{Zr}_x\text{Ti}_{1-x})\text{O}_3$ ceramics were fabricated by the solid state method and sintering at 1300–1350 °C. XRD analysis shows that all the compositions exhibited single perovskite structure without secondary phase. The substitution of Ti^{4+} by Zr^{4+} leads to an expansion of the lattice. The average grain size decreased from 5.21 to 4.03 μm when Zr content increases from $x = 0.05$ to 0.25, respectively. Ferroelectric hysteresis loops at room temperature became slim with Zr-doping. For the composition of $x = 0.25$, the maximum recoverable energy-storage density was 0.2 J/cm³ under 6.7 kV/mm. The modified Curie-Weiss law was applied to describe the diffuse phase transition and relaxor characteristics in the $\text{Ba}(\text{Zr}_x\text{Ti}_{1-x})\text{O}_3$ ceramics. Diffuseness coefficient γ was calculated to be 1.89–1.90 for the ceramics with $x = 0.10$ –0.25. The permittivity of $\text{Ba}(\text{Zr}_x\text{Ti}_{1-x})\text{O}_3$ ceramics at room temperature increased with Zr-doping. For the composition of $x = 0.20$, ε_r was over 10500 at both 1 kHz and 100 kHz.

References

1. R.C. Kell, N.J. Hellicar, “Structural transitions in barium titanate-zirconate transducer materials”, *Acta Acustica United with Acustica*, **6** (1956) 235–245.
2. P.S. Dobal, A. Dixit, R.S. Katiyar, “Micro-Raman scattering and dielectric investigations of phase transition behavior in the BaTiO_3 - BaZrO_3 system”, *J. Appl. Phys.*, **89** [12] (2001) 8085–8091.
3. Z. Yao, H. Liu, Y. Liu, Z. Wu, Z. Shen, Y. Liu, M. Cao, “Structure and dielectric behavior of Nd-doped BaTiO_3 perovskites”, *Mater. Chem. Phys.*, **109** [2-3] (2008) 475–481.
4. H. Kishi, Y. Mizuno, H. Chazono, “Base-metal electrode-multilayer ceramic capacitors: past, present and future perspectives”, *Jpn. J. Appl. Phys.*, **42** [1] (2003) 1–15.
5. B. Zhou, *Preparation and Modification of BaTiO_3 -based Dielectric Ceramics with High Permittivity*, Ph.D. Thesis, Wuhan University of Technology, Wuhan, China, 2015.
6. W. Zhang, S. Xue, S. Liu, J. Wang, B. Shen, J. Zhai, “Structure and dielectric properties of $\text{Ba}_x\text{Sr}_{1-x}\text{TiO}_3$ -based glass ceramics for energy storage”, *J. Alloys Compd.*, **617** (2014) 740–745.
7. C. Xu, Z. Yao, K. Lu, H. Hao, Z. Yu, M. Cao, H. Liu, “Enhanced piezoelectric properties and thermal stability in tetragonal-structured $(\text{Ba,Ca})(\text{Zr,Ti})\text{O}_3$ piezoelectrics substituted with trace amount of Mn”, *Ceram. Int.*, **42** [14]

- (2016) 16109–16115.
8. X. Huang, H. Liu, H. Hao, S. Zhang, Y. Sun, W. Zhang, L. Zhang, M. Cao, “Microstructure effect on dielectric properties of MgO-doped BaTiO₃-BiYO₃ ceramics”, *Ceram. Int.*, **41** [6] (2015) 7489–7495.
 9. B.W. Ricketts, G. Triani, A.D. Hilton, “Dielectric energy storage densities in Ba_{1-x}Sr_xTi_{1-y}Zr_yO₃ ceramics”, *J. Mater. Sci. Mater. Electron.*, **11** (2000) 513–517.
 10. N. Baskaran, H. Chang, “Effect of Sn doping on the phase transformation properties of ferroelectric BaTiO₃”, *J. Mater. Sci. Mater. Electron.*, **12** [9] (2001) 527–531.
 11. M. Kahn, “Influence of grain growth on dielectric properties of Nb-doped BaTiO₃”, *J. Am. Ceram. Soc.*, **54** [9] (1971) 455–457.
 12. V. Tura, L. Mitoseriu, “Ageing of low field dielectric constant and losses in (Hf,Zr)-doped BaTiO₃ ceramics”, *Europhys. Lett.*, **50** [6] (2000) 810–815.
 13. M.F. Islam, R. Mahbub, A. Mousharraf, “Effect of sintering parameters and Ta₂O₅ doping on the microstructure and dielectric properties of BaTiO₃ based ceramics”, *Key Eng. Mater.*, **608** (2014) 247–252.
 14. B. Tang, S. Zhang, Y. Yuan, X. Zhou, “Latest progress of curie point shift of barium titanate ceramic and its mechanisms”, *Chin. J. Vacuum Sci. Technol.*, **2008** [2] (2008) 120–125.
 15. R.D. Shannon, “Revised effective ionic radii and systematic studies of interatomic distances in halides and chalcogenides”, *Acta Crystallogr.*, **32** [5] (1976) 751–767.
 16. K.M. Sangwan, N. Ahlawat, R.S. Kundu, S. Rani, S. Rani, N. Ahlawat, S. Murugavel, “Improved dielectric and ferroelectric properties of Mn doped barium zirconium titanate (BZT) ceramics for energy storage applications”, *J. Phys. Chem. Solids*, **117** (2018) 158–166.
 17. Y. Li, R. Wang, X. Ma, Z. Li, R. Sang, Y. Qu, “Dielectric behavior of samarium-doped BaZr_{0.2}Ti_{0.8}O₃ ceramics”, *Mater. Res. Bull.*, **49** (2014) 601–607.
 18. X. Wang, Z. Zheng, S. Yan, J. Luo, P. He, Y. Xing, “Effects of Sm₂O₃ doping on the dielectric properties of barium zirconium titanate ceramics”, *China Ceram.*, **52** [6] (2016) 53–56.
 19. H. Zhai, *Preparation and Dielectric Properties of Ba(Zr_xTi_{1-x})O₃ Powders and Ceramics by Sol-Gel Process*, Ph.D Thesis, Qingdao University, China, 2007.
 20. Y. Xu, *Preparation and Modification of Barium Zirconate Titanate Ceramics*, Ph.D. Thesis, Shaanxi University of Technology, China, 2019.
 21. N.H. Fletcher, A.D. Hilton, B.W. Ricketts, “Optimization of energy storage density in ceramic capacitors”, *J. Phys. D Appl. Phys.*, **29** [1] (1996) 253–258.
 22. Q. Xu, M.T. Lanagan, X. Huang, J. Xie, L. Zhang, H. Hao, H. Liu, “Dielectric behavior and impedance spectroscopy in lead-free BNT-BT-NBN perovskite ceramics for energy storage”, *Ceram. Int.*, **42** [8] (2016) 9728–9736.
 23. H. Ogihara, C.A. Randall, S. Trolier-Mckinstry, “High-energy density capacitors utilizing 0.7BaTiO₃-0.3BiScO₃ ceramics”, *J. Am. Ceram. Soc.*, **92** [8] (2009) 1719–1724.
 24. S. Chen, X. Wang, T. Yang, J. Wang, “Composition-dependent dielectric properties and energy storage performance of (Pb,La)(Zr,Sn,Ti)O₃ antiferroelectric ceramics”, *J. Electroceram.*, **32** [4] (2014) 307–310.
 25. Z. Song, H. Liu, S. Zhang, Z. Wang, Y. Shi, H. Hao, M. Cao, Z. Yao, Z. Yu, “Effect of grain size on the energy storage properties of (Ba_{0.4}Sr_{0.6})TiO₃ paraelectric ceramics”, *J. Eur. Ceram. Soc.*, **34** [5] (2014) 1209–1217.
 26. T. Wu, Y. Pu, K. Chen, “Dielectric relaxation behavior and energy storage properties in Ba_{0.4}Sr_{0.6}Zr_{0.15}Ti_{0.85}O₃ ceramics with glass additives”, *Ceram. Int.*, **39** [6] (2013) 6787–6793.
 27. M. Kuwabara, H. Matsuda, “Shift of the curie point of barium titanate ceramics with sintering temperature”, *J. Am. Ceram. Soc.*, **80** [10] (1997) 2590–2596.
 28. S. Mahajan, D. Haridas, K. Sreenivas, O.P. Thakur, C. Prakash, “Enhancement in electro-strain behavior by La³⁺ substitution in lead free BaZr_{0.05}Ti_{0.95}O₃ ceramics”, *Mater. Lett.*, **97** (2013) 40–43.
 29. Z. Wang, M. Cao, Q. Zhang, H. Hao, Z. Yao, Z. Wang, Z. Song, Y. Zhang, W. Hu, H. Liu, “Dielectric relaxation in Zr-doped SrTiO₃ ceramics sintered in N₂ with giant permittivity and low dielectric loss”, *J. Am. Ceram. Soc.*, **98** [2] (2014) 476–482.
 30. C.C. Jin, F.F. Wang, Q.R. Yao, Y.X. Tang, T. Wang, W.Z. Shi, “Ferroelectric, dielectric properties and large strain response in Zr-modified (Bi_{0.5}Na_{0.5})TiO₃-BaTiO₃ lead-free ceramics”, *Ceram. Int.*, **40** [4] (2014) 6143–6150.